

# Falling ball viscosimetry of giant vesicle membranes: Finite-size effects

R. Dimova<sup>1,2</sup>, C. Dietrich<sup>1,a</sup>, A. Hadjiisky<sup>1,2</sup>, K. Danov<sup>2</sup>, and B. Pouligny<sup>1,b</sup>

<sup>1</sup> Centre de recherche Paul-Pascal, CNRS, avenue A. Schweitzer, 33600 Pessac, France

<sup>2</sup> Laboratory of Thermodynamics and Physico-Chemical Hydrodynamics, Faculty of Chemistry, University of Sofia, 1164 Sofia, Bulgaria

Received 4 January 1999 and Received in final form 11 May 1999

**Abstract.** We study the general problem of the friction felt by a spherical solid particle which moves parallel to the membrane of a spherical vesicle. Experiments are carried out with SOPC vesicles at room temperature, with different particle and vesicle sizes. Experimental data show considerable finite-size effects whenever the particle is not very small compared to the vesicle. These effects are found consistent with the hydrodynamical theory of the vesicle-particle problem. This agreement allows for a “robust” determination of membrane viscosity, independently of particle and vesicle sizes.

**PACS.** 68.10.Et Interface elasticity, viscosity, and viscoelasticity – 83.85.Pt Flow computation (e.g. finite element)

## 1 Introduction

Phospholipid bilayers are used in a wide variety of experiments as ultimately simplified models of cell membranes. Much work has been done in the past two decades to quantitatively characterize basic mechanical and hydrodynamical properties of model membranes [1]. Among these, the membrane shear viscosity,  $\eta_S$ , is believed to play a crucial role in controlling the motion of membrane inclusions [2] and dynamic cell deformation [3].

Basically,  $\eta_S$  is a macroscopic quantity which can be defined only on scales much larger than structural details of the membrane [4]. There have been attempts to estimate membrane viscosities from translational and rotational Brownian motions of molecules in membranes, by fluorescence or nuclear magnetic resonance techniques [2]. Because of the microscopic character of the probe in these experiments, such techniques do not allow to measure a true viscosity but only a microscopic probe-dependent quantity, sometimes termed a “microviscosity”. Estimates for different phospholipid bilayers in the fluid state,  $L_\alpha$ , are on the order of  $10^{-7}$  or  $10^{-6}$  surface poises (sp) [3, 5, 6]. A macroscopic technique was proposed by Waugh [3], whose principle was to pull a filament out of a giant vesicle. Interpretation of experimental data by means of a model proposed by the author led to estimating shear viscosities of egg phosphatidylcholine membranes in the  $10^{-6} \div 10^{-4}$  sp range. The considerable dispersion of re-

sults was attributed to the multilamellarity of the vesicle preparation. The lower boundary for  $\eta_S$  from Waugh’s data was about  $5 \times 10^{-6}$  sp.

Recently, our group proposed a new method using a solid microsphere as a macroscopic mechanical probe to “feel” the viscosity of a fluid membrane [7]. In our procedure, the lipid bilayer is in the form of a spherical giant vesicle (radius  $R$ ,  $10 \leq R \leq 50 \mu\text{m}$ ). The particle, a polystyrene or glass microsphere (radius  $a$ ,  $0.8 \leq a \leq 10 \mu\text{m}$ ) is manipulated by means of an optical trap and brought in contact with the vesicle. Usually the particle adheres to the membrane, with a finite contact angle ( $\alpha$ ), as shown in Figure 1a. If the membrane is in the fluid state, the particle can still be moved along the vesicle contour by means of the optical trap. In our experiments, we bring the particle near the top of the vesicle and release it by switching off the laser beams. Then it starts moving down, as shown in Figure 1c.

In [7] we showed preliminary results obtained with polystyrene particles and SOPC ( $L_\alpha$ -stearoyl-oleyl-phosphatidylcholine) giant vesicles at room temperature. We measured the friction ( $\zeta$ ) felt by such particles moving along the surfaces of the vesicles and proposed an approximate procedure to find the value of  $\eta_S$  from that of  $\zeta$ . This procedure was based on an adaptation of Danov *et al.*’s theory [8] for a spherical particle straddling a viscous film at the water-air interface, supposed flat and infinite. The data were restricted to particles about  $4 \mu\text{m}$  in diameter, and whose equilibrium positions were definitely across the vesicle membrane. This choice was a trade-off between opposite requirements: the particles were large enough to follow definite sedimentation paths (see Sect. 2), which

<sup>a</sup> *Current address:* Department of Cell Biology and Anatomy, University of North Carolina, Chapel Hill, NC-27599, USA.

<sup>b</sup> e-mail: pouligny@crpp.u-bordeaux.fr

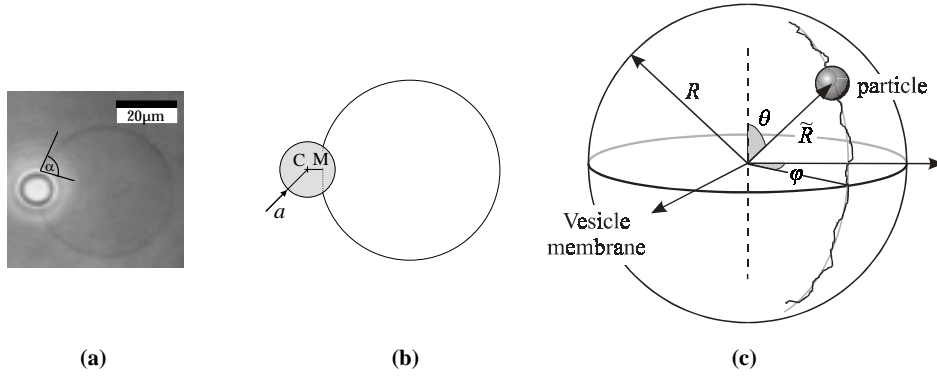


**Fig. 1.** (a) Example of a latex particle attached to a giant SOPC vesicle. The apparent composite structure of the particle (black and white circular zones) is an artifact due to phase contrast microscopy. (b) Definition of particle penetration (see Eq. (1)). (c) Schematic representation of a particle trajectory on the vesicle surface.

allowed for a straightforward determination of  $\zeta$ . On the other hand, they were small enough ( $a/R \leq 0.1$ ) for the approximation of a flat infinite interface to be acceptable. The smallness of the size ratio ( $a/R$ ) and the fact that the contact angle was not too far from  $90^\circ$  were required conditions in the adaptation of Danov *et al.*'s theory.

In this paper, we address the vesicle-particle problem in the most general way, with no restriction on the particle size and position. As we will see, the finiteness of the vesicle size greatly influences the friction felt by large particles. We interpret our results by means of the full hydrodynamical theory of the vesicle-particle problem [9] and arrive at a “robust” (*i.e.* independent of particle size) determination of the membrane shear viscosity.

The paper is organized as follows: in Section 2, we briefly describe our experimental procedure, from sample preparation to particle path analysis and determination of particle friction. Results (in terms of measured frictions) obtained with polystyrene particles, from about 1 to 10  $\mu\text{m}$  in radius, and SOPC vesicles at room temperature, are given in Section 3. Section 4 is on theory and extraction of the membrane shear viscosity from measured frictions. This section does not dwell deeply on the theory hardware, which is the matter of a dedicated paper [9]. Instead, we just state the basic assumptions and definitions, and outline the numerical results of direct interest to our application. Our results (in terms of  $\eta_S$  values) are discussed in Section 5. Main features of this work are summarized in Section 6.

## 2 Experimental procedure

### 2.1 Sample

The vesicles are prepared using the electroformation method [10], in an optical glass cuvette. Details about the cell geometry can be found in [11]. Electrodes are made of two horizontal parallel platinum wires. Electroformation generates a cluster of vesicles of different sizes. Spherical giant vesicles are found in the outer region of this cluster. Such vesicles have their rear sides connected to the cluster apparently through a few points (hard sphere contacts) or, in some cases, by definite contact zones. These show up in the microscope image as zones of low curvature and high contrast.

We select a giant vesicle for experimenting with a microsphere. In general, we eliminate vesicles containing well visible substructures (smaller vesicles or lipid aggregates). An unusually large contrast of the vesicle contour is an indication of multilamellarity and results in rejection too.

After a vesicle has been selected, a small volume of a latex particle suspension (again see [11] for details) is injected far (about 20 mm) from the electrodes. There, a particle is picked up by means of a long-working-distance optical trap [12] and is conveyed to the cluster region. Before contact with the cluster, we perform a calibration experiment to measure the particle friction in bulk water ( $\zeta_0$ ), following the procedure described in Section 2.2. Afterwards, the particle is brought in contact with the outer side of the selected vesicle, near the vesicle “equator” (see Fig. 1c). As described in [11], the particle jumps out of the optical trap and adheres to the lipid membrane. Usually, it stabilizes itself across the vesicle contour with a finite contact angle ( $\alpha$ ). Adhesion dynamics may feature different steps [11], but after equilibrium has been reached  $\alpha$  takes on a constant value (see Fig. 1a). This value is not universal, as it depends much on the initial vesicle tension and the nature of the particle surface. Since SOPC membranes are fluid at room temperature, the particle can be moved along the vesicle surface by means of the optical trap. We release it at some point ( $\theta_0, \varphi_0$ ) (see Fig. 1 for the definition of polar angles) by switching off the laser trap. Afterwards, the particle starts moving, under the influence of gravity and thermal agitation.

The intersection of the vesicle contour with the particle defines a contact line. Experiments carried out by Dietrich *et al.* [11] on “3-body” systems, either a particle with 2 vesicles or 2 particles on a single vesicle, indicate that the contact line is “pinned” [13] to the particle surface. A consequence of contact-line-pinning is that the particle cannot move radially ( $\alpha$  is constant) and can rotate only around the radial axis ( $\vec{R}$  in Fig. 1c). Rolling motion, *i.e.* around an axis perpendicular to  $\vec{R}$ , is forbidden.

The particle-vesicle configuration can be defined by  $\alpha$ , but we prefer to measure the penetration ( $Z$ ) of the particle across the membrane, because this is the parameter most directly felt by the experimentalist.  $Z$  is defined by:

$$Z = 1 - \frac{CM}{a}, \quad (1)$$

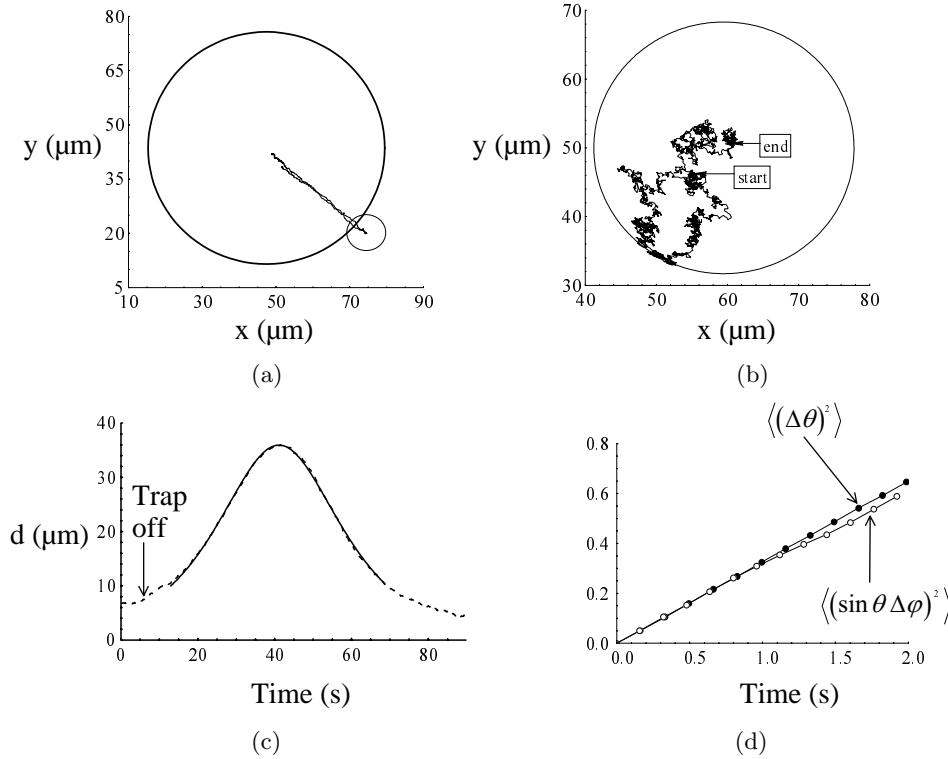


**Fig. 2.** Examples of particle trajectories. (a) Heavy particle ( $a = 5.9 \mu\text{m}$ ,  $R = 32.1 \mu\text{m}$ ,  $Pe = 35\,000$ ). (b) Brownian particle ( $a = 0.8 \mu\text{m}$ ,  $R = 18.3 \mu\text{m}$ ,  $Pe = 50$ ). (c) The heavy particle path is well fitted to by the sedimentation equation (Eq. (3) in text). (d) Statistical analysis of the Brownian particle path.

where  $CM$  is the distance between the plane containing the membrane-particle contact line and the particle center (see Fig. 1b).  $CM$  is positive when  $C$  is exterior to the vesicle and negative otherwise.  $Z$  varies between 0 and 2. These limits correspond to the particle being tangent to the vesicle, externally and internally, respectively.  $Z = 1$  means that the particle center is exactly on the vesicle contour.  $Z$  is measured within  $\pm 5\%$  for the largest particles ( $a \approx 10 \mu\text{m}$ ). The error increases much when  $a$  decreases: with small particles ( $a \approx 1 \mu\text{m}$ ), we cannot do better than discerning outside ( $0 \leq Z \leq 1$ ), medium ( $Z \cong 1$ ) and inside ( $1 \leq Z \leq 2$ ) particle positions.

## 2.2 Particle trajectories

### 2.2.1 Recording

The sample is observed from above through the upper microscope objective of the optical trap [12], either in amplitude or phase contrast. Images are captured by a CCD camera and digitized (8 bits at video rate). A focussed image of a latex particle features a bright central zone. A tracking software (I2S) determines the coordinates  $(x, y)$  of the center of mass of this zone every 4 video frames. The error in  $x$  or  $y$  is about  $\pm 0.2 \mu\text{m}$  [14]. Basically, we record a projection of the particle path in the vesicle equatorial plane. It is not possible to automatically track a particle from top to bottom of a giant vesicle, because it progressively gets out of focus when losing altitude. For this reason, it is necessary to re-adjust the vertical position of the sample cuvette a few times during particle motion; the full sedimentation trajectory is obtained by assembling the corresponding recorded tracks. Two examples of

trajectories are shown in Figures 2a and 2b, for a large ( $a = 5.9 \mu\text{m}$ ) and a small ( $a = 0.8 \mu\text{m}$ ) particle, respectively. There is very few Brownian noise in Figure 2a. The large particle essentially follows a meridian of the vesicle: this is an example of a nearly pure sedimentation path. Conversely, the path in Figure 2b is dominated by Brownian excursions, *i.e.* particle diffusion.

### 2.2.2 Analysis

In the pure sedimentation limit, the particle trajectory is the solution of the simple mechanical equation of motion:

$$\tilde{m}g \sin \theta = \zeta \tilde{R} \frac{d\theta}{dt}. \quad (2)$$

Here  $\tilde{m}g$  is the particle weight corrected for buoyancy,  $\theta$  is the polar angle defined in Figure 1c,  $t$  is the time and  $\tilde{R}$  is the distance between the vesicle and particle centers. Inertia is neglected because of the very small sizes and velocities involved in experiments. Equation (2) is easily integrated in spherical coordinates and gives:

$$f[\theta(t)] = f(\theta_0) - \frac{t}{\tau}, \quad (3)$$

where  $\tau = \tilde{R}\zeta/\tilde{m}g$  is the characteristic time of sedimentation and  $f(\theta) = a \tanh(\cos \theta)$ .

Figure 2c shows the distance of the particle to the  $z$  axis,  $d = \tilde{R} \sin \theta$ , as a function of time, for the example of Figure 2a. The solid line is obtained by fitting equation (3) to the experimental points. The agreement is excellent and gives  $\tau = 14.7$  s within  $\pm 1.5\%$ .

The relevant quantity for membrane viscosimetry is the ratio of  $\zeta$ , the friction felt by the particle bound to the vesicle, to the reference friction,  $\zeta_0 = 6\pi\eta a$  in bulk water ( $\eta$  is the viscosity of water). In the calibration experiment, we measure the sedimentation velocity of the particle in bulk water:  $v_S = \tilde{m}g/\zeta_0$ . The procedure is as follows: after particle release from the optical trap at time  $t_0$  and altitude  $z_0$ , the sample cuvette is moved vertically (lifted up) to bring a different plane,  $z_1$ , in focus [15]. We measure the instant  $t_1$  at which the particle passes through this plane, and repeat the procedure for different planes. We thus build  $z(t)$ , the particle sedimentation trajectory in bulk water. A linear fit then gives  $v_S = dz/dt$ . With a large particle, such as that in Figure 2a,  $v_S$  is measured within  $\pm 0.5\%$ . In this example,  $\bar{\zeta} = \zeta/\zeta_0 = v_S\tau/\tilde{R}$  is found = 1.3.

In the case of a small particle (Fig. 2b), large Brownian excursions make the determination of  $\tau$  and  $v_S$  very difficult, if not impossible. The friction is more conveniently found from the particle translational diffusion coefficient,  $D$ , through the Einstein relation,  $D = k_B T/\zeta$  (here  $k_B$  is the Boltzmann constant and  $T$  is the absolute temperature). Let  $\Delta\varphi_i = \varphi - \varphi_i$  and  $\Delta\theta_i = \theta - \theta_i$  be the excursions of the particle position around a point  $(\theta_i, \varphi_i)$  of the trajectory in a time interval  $\Delta t$ . We expect:

$$\langle(\Delta\theta)^2\rangle = \langle[(\sin\theta)\Delta\varphi]^2\rangle = \frac{2D}{R^2}\Delta t, \quad (4)$$

in the  $\Delta t \rightarrow 0$  limit. In equation (4), the averages are calculated on a single path, by summation on the ensemble of couples  $(\Delta\theta_i, \Delta\varphi_i)$  corresponding to a given  $\Delta t$  [16]. Figure 2d shows the result of this analysis for the example of Figure 2b. Both second order moments,  $\langle(\Delta\theta)^2\rangle$  and  $\langle(\sin\theta\Delta\varphi)^2\rangle$  converge to a common linear behavior for  $\Delta t \leq 1$  second, giving  $D = 0.16$  ( $\mu\text{m}^2/\text{s}$ ). In the calibration procedure, we observe the Brownian motion of the particle in bulk water. We analyze the horizontal excursions in the same way, to find the reference diffusivity  $D_0$ :

$$\langle(\Delta x)^2\rangle = \langle(\Delta y)^2\rangle = 2D_0\Delta t \quad (5)$$

in the  $\Delta t \rightarrow 0$  limit. For small particles, about  $1 \mu\text{m}$  in radius,  $D_0$  and  $D$  are found within  $\pm 5\%$ . The relative friction, which is simply  $\bar{\zeta} = D_0/D$ , is thus measured within  $\pm 10\%$ .

The two examples shown in Figure 2 correspond to a ‘‘heavy’’ (Fig. 2a) and a Brownian (Fig. 2b) particle. In Figure 2a, the motion is driven essentially by  $g$ , with a small thermal noise. The motion in Figure 2b is essentially thermal noise, with a slow drift caused by  $g$ . For particles of intermediate sizes ( $a \approx 2 \mu\text{m}$ ), both mechanisms influence much the particle motion. When the particle moves in a homogeneous unbounded medium (bulk water in our situation), the average particle path,  $\langle r(t) \rangle$ , coincides with the sedimentation path,  $z_S(t) = v_S(t - t_0)$  [17]. In other words, averaging results in decoupling sedimentation and Brownian motion, which makes the measurement of  $v_S$  straightforward. When the particle motion is restrained to the surface of a sphere, the situation is more complex because the average path, which we may define as

$\langle f[\theta(t)] \rangle$ , does not coincide with the sedimentation path,  $f_S(t)$  (given by Eq. (2) right-hand side) [7,18]. In practice, this means that equation (2) cannot be fitted to the particle mean path whatever  $\theta$  in general. Fortunately,  $\langle f[\theta(t)] \rangle$  coincides *approximately* with  $f_S(t)$  near  $\theta = \pi/2$  (the vesicle equator), provided that the particle be ‘‘heavy enough’’ [7,18]. The particle ‘‘heaviness’’ is measured by the parameter  $Pe = \tilde{m}g\tilde{R}/k_B T$ , which is the Peclet number in our problem. We find that  $\tau$  can be found within a few percent using equation (2) whenever  $Pe \geq 100$ . With latex particles, this means  $a \geq 2 \mu\text{m}$ . With smaller particles, analysis of the Brownian motion (Eq. (3)) is preferable because the experimental error on  $D$  is smaller than that on  $\tau$ .

### 3 Results

We measured reduced frictions,  $\bar{\zeta}$ , for particle radii between  $0.8$  and  $10 \mu\text{m}$  and vesicle radii between  $12$  and  $53 \mu\text{m}$ . Results are shown in Figure 3a as  $\bar{\zeta}$  *versus*  $Z$ , for different  $R/a$  ratios. Results for ingested particles ( $Z = 2$ ) are outlined in Figure 3b.

Values of  $\bar{\zeta}$  range from about  $(1.2 \pm 0.1)$  to  $(3.4 \pm 0.1)$ . In spite of a large scatter, examination of the graphs leads to identifying two main trends:

- *Particle much smaller than the host vesicle* (say  $R/a \geq 7$  in Fig. 3a): the particle feels a small increase in hydrodynamic drag between water and the situation across a vesicle membrane. The excess friction,  $\bar{\zeta}^{\text{exc}} = \bar{\zeta} - 1$ , is about  $0.3$  (within  $\pm 30\%$ ), with no obvious dependence on the particle penetration. There is only a slight increase of  $\bar{\zeta}$  near  $Z = 2$ .
- *Large particles* (say  $R/a \leq 7$  in Fig. 3a): in this case, the friction depends very much on  $Z$ . When the particle is outside the vesicle ( $Z \cong 0$ ),  $\bar{\zeta}$  is about the same as with small particles. But  $\bar{\zeta}$  is considerably larger (up to about  $3.5$ ) in the opposite situation of an ingested particle ( $Z \cong 2$ ). This tendency obviously increases when  $R/a$  decreases, as shown in Figure 3b for the case of ingested particles.

To summarize, we observe that  $\bar{\zeta}$  is minimum when the particle is very small compared to the vesicle size, independently of the penetration. Larger particles feel the finite size of the vesicle in the form of a larger friction. This finite-size effect increases much when the particle penetrates more into the vesicle interior.

## 4 Data inversion

### 4.1 Small particles

The  $a/R \rightarrow 0$  limit corresponds to a spherical particle straddling a flat infinite viscous interface, in contact with a 3-dimensional viscous fluid on both sides. In Figure 4, we term this situation the W-W case.

In [8] (which we will refer to as DADL), Danov *et al.* solved this kind of problem for a particle across a film at

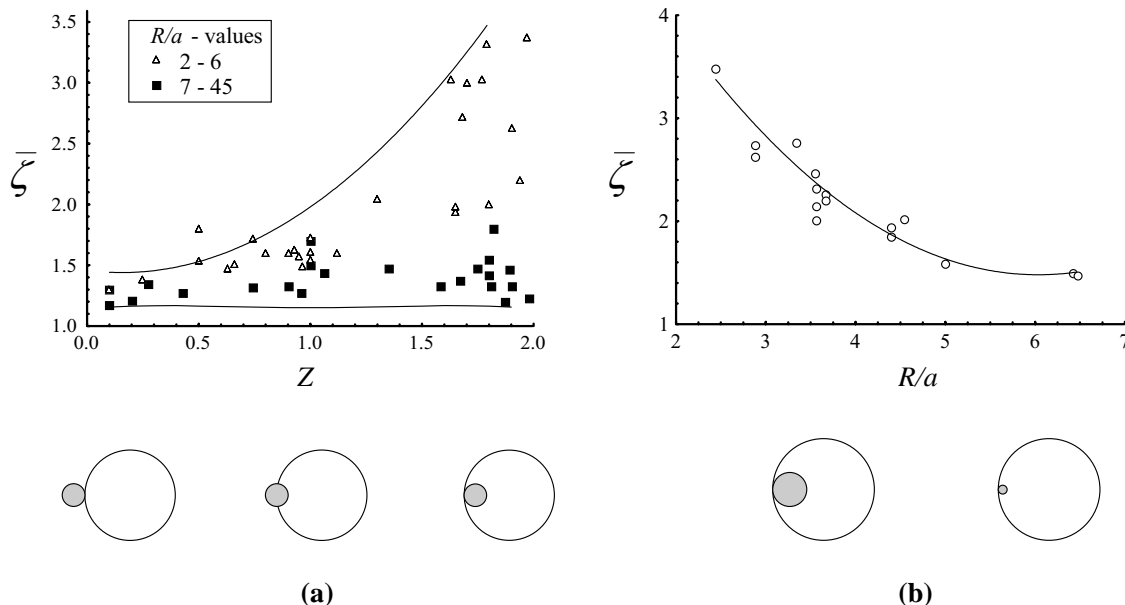


**Fig. 3.** Experimental results. (a) Reduced particle friction versus penetration. Sketches below the graph show the  $Z = 0, 1$  and  $2$  positions for constant  $a$  and  $R$ . The data set is split in 2 subsets: small particles (filled squares) and large ones (open triangles). The top solid line is just a guide to show the increase in  $\bar{\zeta}$  with  $Z$ . The bottom line is  $\bar{\zeta}_{\text{th}}(Z)$  in the  $R/a \rightarrow \infty$  limit for  $E = 1$  (see Sect. 4.2). (b) Reduced friction for fully penetrated particles ( $Z = 2$ ), versus the vesicle-particle size ratio. Large particles (left end of the graph and sketch below) feel a much larger friction than small ones (at right). The solid line is just a guide to the eye.

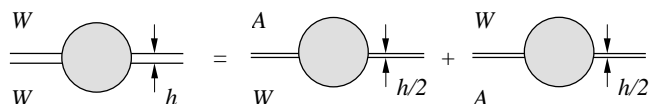


**Fig. 4.** Particle across a flat infinite viscous film. When the contact angle is  $90^\circ$ , simple symmetry allows to find the particle friction in the case of a membrane (WW) from that with a film of half thickness at the water-air (WA) interface.

the water-air interface (denoted W-A or A-W in Fig. 4). Air in this context is a fluid of negligible viscosity, like vacuum. In DADL theory, the contact angle is supposed constant and particle rolling motion is forbidden. The film is infinitely thin, supposed to remain flat during particle motion and the interfacial material (surfactant molecules) is not allowed to slip along the solid particle surface. In other words, surfactant molecules in contact to the particle surface are just stuck to the particle and then do not participate to the membrane flow.

The results of DADL can be applied directly to our problem (W-W) when  $Z = 1$  ( $\alpha = 90^\circ$ ), on the basis of the simple superposition scheme sketched in Figure 4. We denote  $h$  the thickness of the membrane, which we assimilate to a 2-d fluid. In terms of particle friction, the W-W case in Figure 4 is just the superposition of the W-A and A-W situations, with a film of thickness  $h/2$ . This statement can be formulated as:

$$\zeta_{\text{WW}}(h) = 2\zeta_{\text{WA}}(h/2), \quad (6)$$

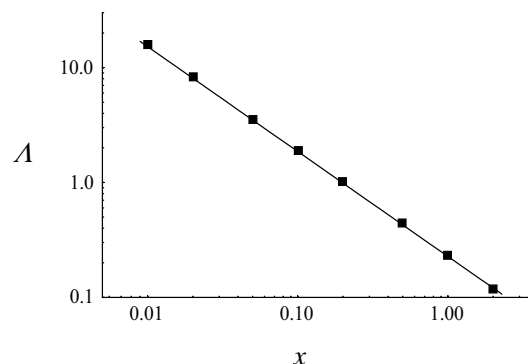


**Fig. 5.** The function  $\Lambda(x)$ , for a spherical particle across a viscous film and a  $90^\circ$  contact angle, in log-log representation. See equation (8) for definition.

for  $Z = 1$ . In DADL, the film is characterized by two dimensionless numbers:

$$E = \frac{\eta_{\text{S,F}}}{\eta a} \quad \text{and} \quad K = \frac{\eta_{\text{D,F}}}{\eta a}, \quad (7)$$

where  $\eta_{\text{S,F}}$  and  $\eta_{\text{D,F}}$  are the film (F) shear and dilation viscosities, respectively. Here we follow the definitions of surface quantities for instance by Edwards *et al.* [19]. Note that surface viscosities have the dimension of a volume viscosity multiplied by a length. Other authors (*e.g.* [20]) prefer to denote such quantities as  $\eta_{\text{m}}h$ , where  $\eta_{\text{m}}$ , either  $\eta_{\text{m,S}} = \eta_{\text{S}}/h$  or  $\eta_{\text{m,D}} = \eta_{\text{D}}/h$ , has the dimension of a bulk viscosity. For our application (lipid bilayers), we will consider the film as incompressible, and then put  $K = 0$ .

It is useful to define a background friction,  $\zeta_{0,\text{WA}} = 3\pi\eta a$  for  $Z = 1$ , and  $\zeta_{0,\text{WW}} = 6\pi\eta a$ , and an excess friction  $\zeta^{\text{exc}} = \zeta - \zeta_0$ . Following the notation introduced by Saffman and by Hughes *et al.* [20], we define the function  $\Lambda$  such that:

$$\zeta_{\text{WA}}^{\text{exc}} = 4\pi\eta a \Lambda\left(\frac{\eta a}{\eta_{\text{S,F}}}\right), \quad (8)$$

for  $Z = 1$ . Since the surface viscosity of the membrane,  $\eta_{\text{S}}$ , is just twice that of the film, equations (6, 8) give:

$$\zeta_{\text{WW}}^{\text{exc}} = 8\pi\eta a \Lambda\left(\frac{2\eta a}{\eta_{\text{S}}}\right) \quad (9)$$

or

$$\bar{\zeta}_{\text{WW}}^{\text{exc}} = \frac{4}{3}\Lambda\left(\frac{2\eta a}{\eta_{\text{S}}}\right), \quad (10)$$

for  $Z = 1$ , as we told. Figure 5 shows a log-log plot of the function  $\Lambda(x)$ , which we built using DADL theory for  $K = 0$ . The plot is nicely fitted to by a simple power law:

$$\Lambda(x) \cong 0.22x^{-0.9}, \quad (11)$$

in the range  $0.005 \leq x \leq 5$ . With  $\eta_{\text{S}} \approx 3 \times 10^{-6}$  sp (we anticipate our final result), the lower boundary (0.005) corresponds to a sphere about ten times larger than the membrane thickness ( $h \cong 4$  nm). Going to smaller particle sizes would not make sense. DADL theory does not apply to particle sizes on the order or smaller than  $h$  (this is so for instance in experiments by Cheung *et al.* with submicron particles in thick soap films [21]). Equations (9,11) yield:

$$\zeta_{\text{WW}}^{\text{exc}} \cong 2.93\eta_{\text{S}} \left(\frac{\eta a}{\eta_{\text{S}}}\right)^{0.1}. \quad (12)$$

It is interesting to compare this result to that of Hughes *et al.* [20] for the friction of a disk of radius  $a$  in the same membrane:

$$\zeta_{\text{Disk}} \cong 4\pi\eta_{\text{S}} \frac{1}{\ln\left(\frac{\eta_{\text{S}}}{\eta a}\right) - \gamma}, \quad (13)$$

when  $\eta a/\eta_{\text{S}} \ll 1$ . In equation (13),  $\gamma$  is Euler's constant ( $= 0.577\dots$ ). Equation (13) shows that  $\zeta_{\text{Disk}}$  depends very few on the disk size, which appears only through a logarithmic correction. As well known, this rather paradoxical result is the consequence of the nearly 2-dimensional character of the membrane-disk problem [20]. As the membrane-sphere problem is nearly 2-d too, we arrive at a similar result, not surprisingly. Equation (13) is an exact analytical result, which is valid in the  $\eta a/\eta_{\text{S}} \rightarrow 0$  limit. Conversely, equation (12) is not an exact expression, but just an approximate representation of a numerical result in a limited range ( $0.005 \ll \eta a/\eta_{\text{S}} \ll 5$ ). Equations (12, 13) have the common characteristic that  $\zeta_{\text{WW}}^{\text{exc}}$  and  $\zeta_{\text{Disk}}$  depend essentially on  $\eta_{\text{S}}$ , while the dependence on  $a$  is just marginal. Nevertheless, notice that equations (12, 13) are

quantitatively different, which means that Saffman's theory for a disk cannot be used to interpret data for spherical particles (much larger than  $h$ , as we told).

We may apply equation (12) to points in Figure 3a corresponding to small particles ( $R/a > 7$ ) well across the vesicle contour ( $Z \cong 1$ ). Reduced frictions are about 1.3 for  $a \cong 1 \mu\text{m}$ , which gives  $\eta_{\text{S}} \cong 2 \times 10^{-6}$  surface poise (sp). As we explained in Section 2, the error on  $\bar{\zeta}$  for small particles is about  $\pm 10\%$ . This results in about  $\pm 30\%$  for the above value of  $\eta_{\text{S}}$ .

## 4.2 General

Values of  $\bar{\zeta}$  for large particles are more accurate, but, as commented in Section 3, they are very sensitive to the finiteness of the vesicle size. To interpret our data in general, we use the recent theory worked out by Danov *et al.* [9] for the motion of a spherical particle bound to a finite-size vesicle, and which we will refer to as DDP. Here we will just state the main physical assumptions made in DDP and which are of direct relevance to our problem. The readers interested in the hardware of the theory are referred to Danov *et al.*'s article [9].

In the same spirit as in the original DADL theory, the contact angle in DDP is supposed constant and particle rolling motion is forbidden. In the general theory, the particle moves along the surface of the vesicle, which is supposed to remain spherical (radius  $R$ ). The fact that the particle motion does not distort the vesicle shape is ensured whenever the vesicle excess area is not too large. Experimentally, we observe that this condition is satisfied with electroformed vesicles. Basically, we see no definite alteration of the vesicle equator shape. Moreover, the adequateness of equation (3) to describe the recorded particle trajectories is a good check that the above hypothesis is correct. On the whole, the supposed constancy of the vesicle spherical shape is correct only within the amplitude of the thermally excited shape fluctuations. As the vesicles used in our experiments have very small excess areas, this amplitude is  $\ll R$ , and then is negligible in the context of our problem.

The theory regards the membrane as a single 2-dimensional fluid, *i.e.* velocity gradients within the membrane and perpendicular to it are forbidden. This means that the theory ignores the possibility for the two monolayers constituting the real membrane to slip relatively to each other. Another assumption is that the membrane material cannot slip along the solid particle surface. This assumption, together with the supposed constancy of the contact angle and the forbidding of particle rolling motion are in line with the experimental observation that the membrane-particle contact line is pinned [11]. With the assumptions made in the model, essentially the above mentioned no-slip condition and the description of the membrane as a single film, the membrane molecules which can move relatively to the particle are only those outside of the contact line, *i.e.* those belonging to the spherical surface of radius  $R$ . In this context, it is not necessary to know how lipids cover the particle surface, in other words,

what is the wetting configuration [11]. Indeed, this is a great simplification.

Coming back to the real system, involving a bilayer instead of a single film, one might make an objection to the theoretical scheme: we may reason assuming the simplest configuration, *i.e.* partial wetting of the particle surface by the membrane [11]. In this situation, only one monolayer (the outer monolayer of the vesicle membrane, say monolayer 1) is in contact with the particle. Only the lipid molecules pertaining to 1 are locked to the particle surface. The lipid molecules pertaining to the other monolayer, say 2, are free to diffuse and, then it is possible that monolayer 2 slips along the particle surface (coated by lipids of 1). In fact, a simple quantitative argument shows that this degree of freedom does not play a significant role in our problem. The argument is based on estimating the friction force,  $F_{\text{slip}}$ , which this slip mechanism would produce on the particle.  $F_{\text{slip}}$  is on the order of  $b_S a^2 V$ , where  $b_S$  is the coefficient of viscous friction between two lipid monolayers [22] and  $V$  the particle velocity. From literature data [6,22], we may put  $b_S \approx 10^6 \text{ dyn s cm}^{-3}$ . The corresponding dimensionless friction coefficient,  $\bar{\zeta}_{\text{slip}} = b_S a^2 / 6\pi\eta a$ , is found  $\approx 10^3$ , at least. Since  $\bar{\zeta}$ , both in experiments and from the theory (see below), is between 1 and 4, we conclude that the slip mechanism has a negligible influence on the particle motion. Thus one may view the bilayer as a single film, as we proposed.

Let us go on with the model. The vesicle-particle system is supposed isolated in space. The friction,  $\zeta$ , is defined as in equation (2), supposing an external force (gravity in Eq. (2)) acting on the particle. The hydrodynamic equations in DDP are similar to those in DADL, but here the phases on both sides of the membrane are made of the same fluid, supposed incompressible and Newtonian (viscosity  $\eta$ ). The vesicle membrane is modeled as a 2-d Newtonian fluid, whose viscous properties are characterized by  $E = \eta_S / \eta a$  and  $K = \eta_D / \eta a$ . The velocity field ( $v$ ) follows the usual Stokes equation in both 3-d media and the Stokes-Boussinesq equation in the membrane [19]. Following the same procedure as in DADL, equations are written in a special curvilinear coordinate system, which allows to transform the initial 3-variable problem ( $v$  and the pressure,  $P$ , depend on 3 space variables) into a 2-variable ( $x_1, x_2$ ) one. Hydrodynamic equations in the ( $x_1, x_2$ ) space are solved numerically using the so-called “alternating-direction-implicit method” [23,24]. The procedure yields the  $v$  and  $P$  fields everywhere in the system, from which the hydrodynamic drag force and torque acting on the particle are computed. Input parameters of the numerical code are  $E$ ,  $K$ ,  $R/a$  and  $Z$ .

In this work, the code was run on a Digital Alpha 3500 workstation. Computing time depends on the values of input parameters and, of course, on the required numerical accuracy. For instance, with  $E = 2$ ,  $K = 0$ ,  $R/a = 5$  and  $Z = 1$ , it took about 2 hours of CPU time to find  $\zeta$  within  $\pm 1\%$ . Bringing  $Z$  close to 0 or 2 makes the computation extremely long (about 48 hours for  $Z = 1.95$ , other inputs unchanged).

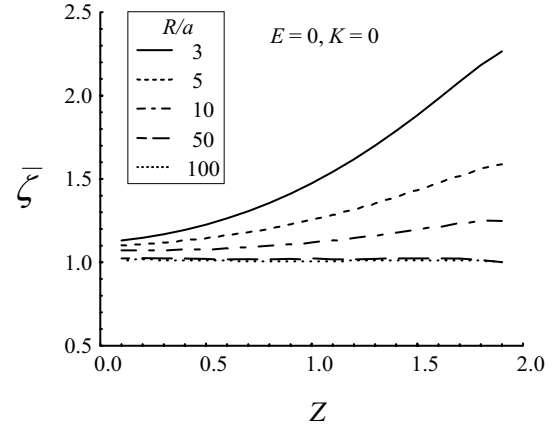


**Fig. 6.** Theoretical friction ratio in the limit of an inviscid vesicle membrane ( $E = K = 0$ ). Finiteness of the vesicle size results in large friction values for large particles, even in the case of a non viscous membrane.

Figure 6 shows results corresponding to  $E = 0$ ,  $K = 0$ , *i.e.* a perfectly inviscid membrane. For very large size ratios ( $R/a = 50, 100$ ), the particle feels nearly no excess friction ( $\bar{\zeta} \cong 1$ ), which is what one might expect intuitively. But with smaller vesicles ( $R/a \leq 10$ ),  $\bar{\zeta}$  is found definitely  $> 1$ : the effect considerably increases when the particle penetrates more into the vesicle and when  $R$  decreases. This is exactly the tendency which we observed experimentally (Fig. 3). The physical reason for the augmented friction is the fact that the portion of the particle inside the vesicle moves in a finite volume. Looping of streamlines inside the volume necessarily increases dissipation. This kind of “re-circulation” effect [25] is obviously highest with a fully penetrated particle ( $Z = 2$ ), but still present when the particle is tangent externally to the vesicle contour ( $Z = 0$ ), because some flow is still excited inside the vesicle through the membrane.

To interpret our data quantitatively, we computed theoretical values of the reduced friction,  $\bar{\zeta}_{\text{th}}$ , corresponding to all experimental parameters,  $R$ ,  $a$  and  $Z$ , for different values of  $\eta_S$  (we kept  $K = 0$  as before). The bottom solid curve in Figure 3a represents  $\bar{\zeta}_{\text{th}}(Z)$  in the  $R \rightarrow \infty$  limit for  $a = 3 \mu\text{m}$ ,  $\eta_S = 3 \times 10^{-6} \text{ sp}$  (this example corresponds to  $E = 1$ ). Clearly this curve fits to the base of the data cloud, where all points correspond to particles about a micrometer in radius. Notice that the curve is nearly flat (except near to  $Z = 0$  or 2), which is what one might expect since the  $R \rightarrow \infty$  limit brings us back to the 2-d problem of the flat infinite membrane.

For a general comparison of computed frictions to experimental ones,  $\bar{\zeta}_{\text{exp}}$ , we plotted the ratio of excess frictions,  $\rho = (\bar{\zeta}_{\text{exp}} - 1) / (\bar{\zeta}_{\text{th}} - 1)$  versus the size ratio  $R/a$ . Results are shown in Figure 7. In this representation, the  $\rho = 1$  line is the master curve where all points should merge, if the model is correct and if a proper value of the adjustable parameter,  $\eta_S$ , has been chosen. Two sets of points are represented, corresponding to  $\eta_S = 3 \times 10^{-6} \text{ sp}$  (filled symbols) and  $7 \times 10^{-6} \text{ sp}$  (open circles).

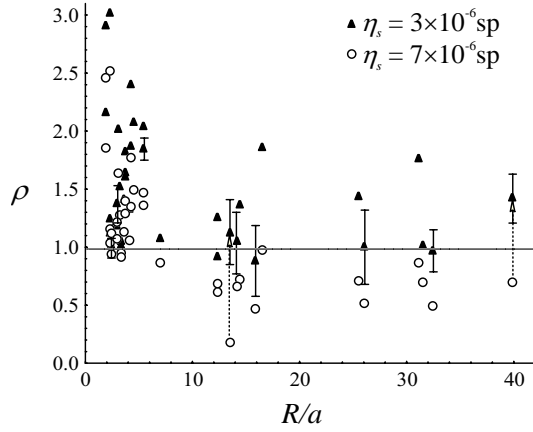


**Fig. 7.** Comparison of experimental ( $\bar{\zeta}_{\text{exp}}$ ) to computed ( $\bar{\zeta}_{\text{th}}$ ) frictions, for different size ratios.  $\rho(\bar{\zeta}_{\text{exp}} - 1)/(\bar{\zeta}_{\text{th}} - 1)$ . Filled triangles correspond to  $\eta_S = 3 \times 10^{-6}$  sp and open circles to  $\eta_S = 7 \times 10^{-6}$  sp. Arrows show the change in  $\rho$  between the 2 values of  $\eta_S$ , for different size ratios.

## 5 Discussion

A striking result of the above analysis is that  $\rho$  values do not gather on the master line, within experimental error and whatever the value of  $\eta_S$ . The obvious conclusion is that the experimental systems are more complex than assumed in the theory. One may infer different kinds of complication, which we already briefly hinted at in Section 2.1:

- (i) bi- or even multi-bilayer membranes;
- (ii) substructures (smaller vesicles, filaments...) attached to vesicle membranes;
- (iii) uncontrolled connections to other vesicles nearby.

One may easily predict that any of these complications will increase the value of  $\zeta$  above that of the ideal system. Hopefully, one may bet that at least a few among our samples were close to ideal and that they correspond to minimal frictions. If this analysis is correct, the ideal systems should be found at the bottom of the data cloud in Figure 7, along the  $\rho = 1$  line. Since there is no relation between particle size and vesicle ideality, ideal systems, if not exceptional, should be found for very different  $R/a$  ratios, and then define a rather straight horizontal boundary at the bottom of the data cloud. This is our criterion to decide what value of  $\eta_S$  best fits to our data. Clearly,  $\eta_S = 3 \times 10^{-6}$  sp does well, while the other value,  $7 \times 10^{-6}$  sp does not.

To explain the anomalies in the data set, we have to estimate the impacts of the above listed complications on particle friction:

- (i) *Multilamellarity*: in 82, Waugh [3] pioneered the field of lipid membrane viscosimetry with a technique based on pulling a filament out of a vesicle. Analysis of his data set led him to estimating only a lower boundary of the surface viscosity,  $\eta_{S,\text{min}}$ , exactly as in our case. Waugh argued that the multi-layer structures of most his vesicles were the reason for the very

large scatter (up to a factor of 30) of  $\eta_S$  values above  $\eta_{S,\text{min}}$ . We doubt that this explanation hold in our situation, because the presence of many multi-layer vesicles would be signed by a quantification of frictions. Notice that most of anomalously large frictions are found with large particles (small  $R/a$  ratios), for which the accuracy in  $\zeta$  is highest. A discretization of  $\rho$  would be beyond experimental error and then visible in the graph. There is nothing such in Figure 7. However note that the absence of a visible discretization of  $\rho$  does not mean that all our vesicles were unilamellar. We just state that multi-lamellarity alone cannot explain the distribution of  $\rho$  values in Figure 7.

- (ii) *Substructures*: this argument does not hold more. The reason is that localized defects on the membrane should show up as accidents on the particle trajectories. Again with large particles, sedimentation trajectories span a very large domain in  $\theta$  and nothing like an anomalous localized slowing down was detected. Trajectories were conform to equation (3), *i.e.* each particle felt a spatially uniform viscosity.
- (iii) *Connections* to other vesicles: such connections may prevent the vesicle to which the particle is attached from rotating as a whole. Overall rotation is permitted in DDP theory and is a reality in experiments with large particles. This can be realized very simply as follows: suppose that the membrane be extremely viscous, say like a gel in which the particle is trapped. In this situation, the particle just acts as a marker of the vesicle motion. The particle trajectory is the solution of the following equation:

$$\tilde{m}g\tilde{R}\sin\theta = \zeta_{\text{rot}}\frac{d\theta}{dt}. \quad (14)$$

Here  $\zeta_{\text{rot}}$  is the rotational friction coefficient of the (solid) vesicle-particle complex. For simplicity we may suppose the complex to be spherical, which amounts to supposing  $Z = 2$ . In this case,  $\zeta_{\text{rot}}$  is simply equal to  $8\pi\eta R^3$  [25]. Note that equation (14) is equivalent to equation (3), with a particle reduced friction  $\bar{\zeta}_{\infty} = 4R/3a$  (here the subscript  $\infty$  means  $\eta_S \rightarrow \infty$ ).

The value of  $\bar{\zeta}_{\infty}$  is relevant to estimate the importance of vesicle overall rotation in the general situation of a finite viscosity. With small particles (say  $R/a > 10$  in our experiments),  $\bar{\zeta}_{\infty}$  is considerably larger than  $\bar{\zeta}$ : in this case, the picture of the particle shearing the membrane of a globally immobile vesicle is correct. Membrane flow does not propagate far out of the particle position, and then connections on the rear side of the vesicle do not influence the particle motion. With large particles,  $\bar{\zeta}_{\infty}$  remains larger than computed values of  $\bar{\zeta}$  for finite viscosities (as one might expect, since  $\bar{\zeta} \rightarrow \bar{\zeta}_{\infty}$  when  $\eta_S \rightarrow \infty$ ), but their orders of magnitude become comparable. For instance, with  $R/a = 2$ ,  $\eta_S = 3 \times 10^{-6}$  sp, we find  $\bar{\zeta} = 2.5$  and  $\bar{\zeta}_{\infty} = 2.7$ . This means that a large particle both shears the membrane and makes the vesicle rotate as a whole. This is



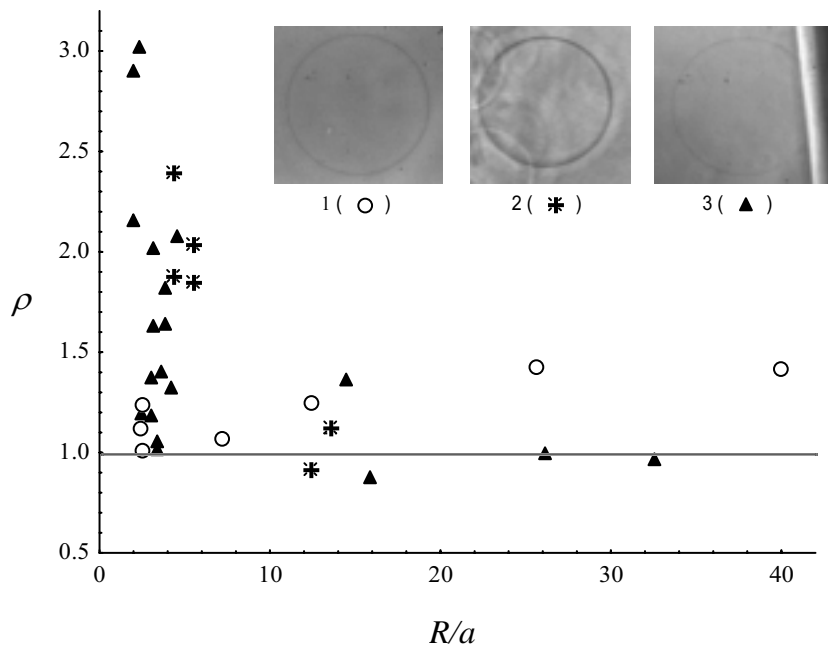


**Fig. 8.** Same data as in Figure 7 for  $\eta_S = 3 \times 10^{-6}$  sp. Analysis in terms of vesicle connectivity: open circles correspond to nearly “ideal” vesicles (example shown in photo 1), asterisks to “connected” spherical vesicles (photo 2) and filled triangles to strongly adhered vesicles (photo 3).

the theoretical scenario, for an ideal system. In a real system such as in the above example, anything which may hinder vesicle rotation will considerably influence the particle trajectory. In practice, the presence of contacts to nearby vesicles may be enough to explain the anomalous values of  $\rho$  in Figure 7.

In the experiment, it is not possible to directly view the contacts between a spherical vesicle and the surrounding ones. The microscope image just shows contours of nearby vesicles which intersect that of the selected one. We may simply bet that the multiplicity of overlapping contours is an indication of the abundance of contacts. We used this rough criterion to discern 2 categories of spherical vesicles in our data, according to their degrees of entanglement with neighbors, or, equivalently, to their degrees of externality relatively to the cluster. Ideal or nearly ideal vesicles (open circles in Fig. 8 and insert photograph 1) are almost free of intersections with neighbor contours; there is even an example of a vesicle which was completely detached from the cluster. In the intermediate category (asterisks and photograph 2), the selected vesicle is partially embedded in the cluster; only the outer portion of the vesicle contour is free of overlaps with neighbors. There is a third category (filled triangles and photograph 3) in Figure 8, which corresponds to vesicles which were non spherical because their rear sides were apparently flat and stuck to the platinum electrode. Figure 8 clearly shows a correlation between anomaly in  $\rho$  and non ideality: highest values of  $\rho$  are found with large particles and vesicles of the above-defined second and third categories. This correlation definitely supports our view that vesicle rotation hindrance is the cause of the problem.

## 6 Conclusion

We studied the problem of falling-ball viscosimetry of giant vesicle membranes, with different particle ( $a$ ) and vesi-

cle ( $R$ ) sizes. A major goal of this study was to determine a value of the membrane shear viscosity ( $\eta_S$ ) that might be termed “robust”, *i.e.* independent of  $a$  and  $R$ . We experimented on SOPC at room temperature, with polystyrene particles of different sizes, for  $0.03 \leq a/R \leq 0.5$ . The friction ( $\zeta$ ) felt by each particle moving on a vesicle surface was determined either from its Brownian motion or from its sedimentation path, depending on the value of the Peclet number.

Experimental results showed that the particle motion was considerably slowed down when the particle was large and penetrated more inside the vesicle. This finding is well in line with the prediction of the recent hydrodynamical theory of the vesicle-spherical particle problem [9]. According to theory, the finiteness of the vesicle size has a twofold effect:

- (i)  $\zeta$  is increased by the re-circulation flow inside the vesicle;
- (ii) the possibility for the vesicle-particle complex (supposed ideal, *i.e.* isolated in water) to rotate as a whole keeps  $\zeta$  within an upper bound,  $\zeta_\infty$ , on the order of  $R/a$ .

We found that both (i) and (ii) are important in our experiments with large particles. Some of the measured frictions were found  $> \zeta_\infty$ , from which we concluded that the overall rotation of the corresponding vesicles was hindered by connections to neighbors.

Data inversion by means of DDP theory [9] led us to selecting a subset of “ideal” vesicles, ideality meaning no indication of multi-layer structure or of overall rotation hindrance. This subset covers the full range of particle sizes, from about 1 to 10  $\mu\text{m}$ , and is consistent with  $\eta_S = 3 \times 10^{-6}$  sp, the value announced in the preliminary work by Velikov *et al.* [7] with small particles ( $a \cong 4 \mu\text{m}$ ). This value is in line with other estimates of model membranes viscosities obtained from other techniques

(see the introduction), in so far as only an order of magnitude comparison is feasible. The error on  $\eta_S$  remains about  $\pm 30\%$  whatever  $a$ , though the accuracy in  $\zeta$  is much better for large particles than for small ones. In fact the gain in accuracy for large  $a$  is counterbalanced by a decreased sensitivity of  $\zeta$  on  $\eta_S$  and by the large scatter due to system non-ideality.

A practical conclusion to be drawn from our data for SOPC is that main artifacts are found with very large particles, say when  $R/a \leq 8$ . It is then recommendable to perform viscosimetry experiments with smaller particles, say  $a \leq 0.1R$ . With very small particles ( $a \leq 1 \mu\text{m}$ ), the procedure to measure  $\zeta$  involves analyzing Brownian trajectories and the particle penetration is hardly measurable. But  $\eta_S$  can be found from  $\zeta$  very simply, using the approximate procedure described in Section 4.1, provided that  $\alpha$  be not far from  $90^\circ$  ( $Z \cong 1$ ) [7]. With larger particles ( $a \approx 2 \mu\text{m}$  or more),  $\zeta$  is measured most directly from sedimentation paths and particle penetrations are well resolved in microscope images. But finite-size effects, essentially re-circulation, significantly increase  $\zeta$ . In this case, extracting the value of  $\eta_S$  implies computing  $\zeta_{\text{th}}$  with the full hydrodynamical theory.

A final – but not least – remark is that whatever the chosen procedure, an absolute value of  $\eta_S$  can be found only from a statistical analysis of data from many different vesicles.

We acknowledge the financial support of the “Laboratoire franco-bulgare” (CNRS/Bulgarian Academy of Sciences-University of Sofia), of ULTIMATECH program (CNRS), of European Union, through Tempus JEP3949 and a fellowship to one of us (C.D.), and the French government for a 3-year Ph.D. grant (R.D.). We thank Claire Lavigne for her data concerning the accuracy of the particle tracking procedure, L. Salomé, P. Méléard, J.-C. Talbot and N. Petrova for useful discussions.

## References

1. See for instance: *Vesicles*, edited by M. Rosoff (Marcel Dekker, New York, Basel, Hong Kong, 1996).
2. See for instance: J.F. Tocanne, L. Dupou-Cezanne, A. Lopez, *Prog. Lipid Res.* **33**, 203 (1994) and references therein.
3. R.E. Waugh, *Biophys. J.* **38**, 19 (1982); *ibid.* **38**, 29 (1982).
4. In this problem, the cut-off length is at least on the order of a lipid molecule width ( $\sim 1 \text{ nm}$ ). It may increase to much larger values near the main transition temperature, because of the dynamic clustering of lipids into gel-like domains. See: O.G. Mouritsen, K. Jorgensen, *BioEssays* **14**, 129 (1992) and references therein.
5. H.J. Galla, W. Hartmann, U. Theilen, E. Sackmann, *J. Membr. Biol.* **48**, 215 (1979); W.L.C. Vaz, R.M. Clegg, D. Hallmann, *Biochemistry* **24**, 781 (1985); W. Birmach, D.D. Thomas, *Biochemistry* **29**, 3904 (1990).
6. R. Merkel, E. Sackmann, E. Evans, *J. Phys. France* **50**, 1535 (1989).
7. K. Velikov, C. Dietrich, A. Hadjiisky, K. Danov, B. Pouligny, *Europhys. Lett.* **40**, 405 (1997).
8. K. Danov, R. Aust, F. Durst, U. Lange, *J. Coll. Interf. Sci.* **175**, 36 (1995).
9. K. Danov, R. Dimova, B. Pouligny (manuscript submitted for publication).
10. M.I. Angelova, D.S. Dimitrov, *Prog. Colloid Polym. Sci.* **76**, 59 (1988); M.I. Angelova, S. Soléau, P. Méléard, J.F. Faucon, P. Bothorel, *Springer Proc. Phys.* **66**, 178 (1992).
11. C. Dietrich, M. Angelova, B. Pouligny, *J. Phys. II France* **7**, 1651 (1997).
12. M.I. Angelova, B. Pouligny, *Pure Appl. Opt. A* **2**, 261 (1993).
13. P.G. de Gennes, *Rev. Mod. Phys.* **57**, 827 (1985).
14. We estimated this error from tests with a particle which was “frozen” inside a water-agarose gel, and moved to different pre-determined positions with a motorized stage.
15. Here  $z$  is the altitude of the observation plane in a frame linked to the cuvette. In practice, we measure  $h$ , the altitude of the cuvette in the laboratory frame.  $vs$  is equal to  $ndh/dt$ , where  $n$  is the refractive index of water ( $\cong 1.34$ ). See: G. Martinot-Lagarde, Ph.D. thesis, Université Bordeaux 1, 1995.
16. H. Qian, M.P. Sheetz, E.L. Elson, *Biophysical J.* **60**, 910 (1991).
17. See for instance: B.J. Berne, R. Pecora, *Dynamic Light Scattering* (John Wiley and Sons, New York, 1976).
18. K. Velikov, K. Danov, M.I. Angelova, C. Dietrich, B. Pouligny, *Colloids Surf. A* **149**, 245 (1999).
19. L.E. Scriven, *Chem. Eng. Sci.* **12**, 98 (1960); D.A. Edwards, H. Brenner, D.T. Wasan, *Interfacial Transport Processes and Rheology* (Butterworth-Heinemann, Boston, 1991).
20. P.G. Saffman, *J. Fluid Mech.* **73**, 593 (1976); B.D. Hughes, B.A. Pailthorpe, L.R. White, *J. Fluid Mech.* **110**, 349 (1981).
21. C. Cheung, Y.H. Hwang, X.I. Wu, H.J. Choi, *Phys. Rev. Lett.* **76**, 2531 (1996).
22. For a general discussion of fluid bilayers viscous modes, see U. Seifert, S.A. Langer, *Europhys. Lett.* **23**, 71 (1993). Experimentally, the value of  $b_S$  can be estimated from the translational diffusion of lipid probes in a single leaflet of a bilayer [6]. Interestingly, pulling a filament out of a vesicle generates a macroscopic monolayer-monolayer friction, which is reflected in the filament growth dynamics. See E. Evans, A. Yeung, R. Waugh, J. Song, *Structure and Conformation of Amphiphilic Membranes*, edited by R. Lipowsky, D. Richter, K. Kremer (Springer, Berlin, 1992), p. 148. Both techniques yield  $b_S$  values between  $10^6$  and  $10^7 \text{ dyn cm}^{-3}$ .
23. C. Pozrikidis, *Introduction to Theoretical and Computational Fluid Dynamics* (Oxford University Press, New York, 1997).
24. K. Danov, R. Aust, F. Durst, U. Lange, *Chem. Eng. Sci.* **50**, 263 (1995).
25. J. Happel, H. Brenner, *Low Reynolds Number Hydrodynamics* (Kluwer Academic Publishers, Dordrecht, Boston, London, 1991); E. Guyon, J.P. Hulin, L. Petit, in *Hydrodynamique physique* (InterEditions/CNRS Éditions, 1994).